A satellite view of aerosols in the climate system

Yoram J. Kaufman*, Didier Tanré† & Olivier Boucher†

*NASA/Goddard Space Flight Center, Greenbelt, Maryland 20771, USA (e-mail: kaufman@climate.gsfc.nasa.gov)
†Laboratoire d'Optique Atmosphérique, Université de Lille/CNRS, Villeneuve d'Ascq, France

Anthropogenic aerosols are intricately linked to the climate system and to the hydrologic cycle. The net effect of aerosols is to cool the climate system by reflecting sunlight. Depending on their composition, aerosols can also absorb sunlight in the atmosphere, further cooling the surface but warming the atmosphere in the process. These effects of aerosols on the temperature profile, along with the role of aerosols as cloud condensation nuclei, impact the hydrologic cycle, through changes in cloud cover, cloud properties and precipitation. Unravelling these feedbacks is particularly difficult because aerosols take a multitude of shapes and forms, ranging from desert dust to urban pollution, and because aerosol concentrations vary strongly over time and space. To accurately study aerosol distribution and composition therefore requires continuous observations from satellites, networks of ground-based instruments and dedicated field experiments. Increases in aerosol concentration and changes in their composition, driven by industrialization and an expanding population, may adversely affect the Earth's climate and water supply.

During the last century, the Earth's surface temperature increased by 0.6 °C, reaching the highest levels in the last millennium[1]. This rapid temperature change is attributed to a shift of less than 1% (ref. 2) in the energy balance between absorption of incoming solar radiation and emission of thermal radiation from the Earth system. Among the different agents of climate change, anthropogenic greenhouse gases and aerosols have the larger roles[1]. Whereas greenhouse gases reduce the emission of thermal radiation to space, thereby warming the surface, aerosols mainly reflect and absorb solar radiation (the aerosol direct effect) and modify cloud properties (the aerosol indirect effect), cooling the surface. These impacts on the radiation balance are very different and therefore require different research approaches.

Greenhouse gases, such as carbon dioxide and methane, have a lifetime of up to 100 years in the atmosphere and a rather homogeneous distribution around the globe; this is in contrast to the heterogeneous spatial and temporal distribution of tropospheric aerosols, which results from their short lifetime of about a week[1,3]. As a consequence, the global increase in the CO_2 concentration of 1–2 p.p.m. per year was measured half a century ago using a single ground-based instrument[4], while daily satellite observations[5,6] and continuous *in situ* measurements[7,8] are needed to observe the emission and transport of dense aerosol plumes downwind of populated and polluted regions (urban haze), regions with vegetation fires (smoke), and deserts (dust). The effect of greenhouse gases on the energy budget occurs everywhere around the globe. Aerosols have both regional and global impacts on the energy budget, requiring frequent global measurements tied to elaborate models that provide realistic representations of the atmospheric aerosols[3,9,10].

Aerosol effects on climate differ from those of greenhouse gases in two additional ways. Because most aerosols are highly reflective, they raise our planet's albedo, thereby cooling the surface and effectively offsetting greenhouse gas warming by anywhere from 25 to 50% (refs 1, 9–11). However, aerosols containing black graphitic and tarry carbon particles (present in smoke and urban haze) are dark and therefore strongly absorb incoming sunlight. The effects of this type of aerosol are twofold, both warming the atmosphere and cooling the surface before a redistribution of the energy occurs in the column. During periods of heavy aerosol concentrations over the Indian Ocean[12] and Amazon Basin[13], for example, measurements revealed that the black carbon aerosol warmed the lowest 2–4 km of the atmosphere while reducing by 15% the amount of sunlight reaching the surface. Heating the atmosphere and cooling the surface below reduces the atmosphere's vertical temperature gradient and therefore is expected to cause a decline in evaporation and cloud formation[14,15].

The second way in which aerosols differ from greenhouse gases is through the aerosol effect on clouds and precipitation. In polluted regions, the numerous aerosol particles share the condensed water during cloud formation, therefore reducing cloud droplet size by 20–30%, causing an increase in cloud reflectance of sunlight by up to 25% (refs. 2, 16–19), and cooling the Earth's surface. The smaller, polluted cloud droplets are inefficient in producing precipitation[20,21], so they may ultimately modify precipitation patterns in populated regions that are adapted to present precipitation rates. The cooling effect due to polluted clouds is still poorly characterized with an uncertainty 5 to 10 times larger than the uncertainty in the predicted warming effect of greenhouse gases[1,22]. The effect of aerosols on precipitation is even less well understood.

To assess the aerosol effect on climate we first need to distinguish natural from anthropogenic aerosols. Satellite data and aerosol transport models show that plumes of smoke and regional pollution have distinguishably large concentrations of aerosols in particular of fine (submicron) size. In contrast, natural aerosol layers may have concentrated coarse dust particles and only widespread fine aerosols from oceanic and continental sources[23]. The ability of satellites to observe the spatial distribution of aerosols[24–28], and to distinguish fine from coarse particles, can be exploited to separate natural from anthropogenic aerosols. *In situ* measurements of aerosol composition[29,30] and size, models that assimilate

the measurements and information on population density and economic activities are needed to further quantify the anthropogenic aerosol component, and to relate it to specific sources.

Aerosol research is in transition from an exploratory phase to a global quantitative phase. The exploratory phase is dominated by the discovery of new aerosol-related processes. For example, the large concentration of black carbon emitted from vegetation fires and found in regional pollution in the tropics[31–33] and its effect on slowing down the hydrologic cycle[2,34]; or the effect of aerosol on reducing precipitation efficiency[20,21,35,36] and counteracting regionally the greenhouse warming[9,10,17]. In this phase, models are used to assess the potential of aerosol processes to affect the global climate[10,37]. Because aerosols vary widely from region to region, a multiple-measurement approach is necessary to assess their impacts on global climate. Specifically, we require the use of long-term, detailed global measurements from satellites[17,23,38–40], distributed networks of ground-based instruments[29,41,42], and comprehensive regional experiments in clean[43] and polluted[31,32] environments, that feed global aerosol and climate models[14,23,44].

Regional variability of aerosols

Most aerosols are regional in nature owing to their short lifetime, the regional distribution of sources, and the variability in their properties. Seasonal meteorological conditions determine how far aerosols are transported from their sources as well as how distributed they are vertically through the atmosphere. Elevated aerosol layers can be picked up by strong winds and transported from Africa or Asia to America and from America to Europe[7,8]. Aerosol properties are modified during the transport by dry or wet deposition, in-cloud processes, and atmospheric chemical reactions.

Aerosol optical thickness (AOT) describes attenuation of sunlight by a column of aerosol, and thus serves as a measure of aerosol column concentration. In Fig. 1a,b, AOT is shown separately for fine and coarse aerosol for September 2000, using satellite techniques discussed in Box 1; several typical regional aerosols are distinguished (see also Table 1).

Urban and industrial regional pollution (urban haze)

These mainly fine hygroscopic particles are found downwind of populated regions[5] (regions a, c and e in Fig. 1a) in air polluted, for example, by car engines, industry, cooking and fireplaces. In China, economic growth and population expansion increased AOT from 0.38 in 1960 to 0.47 in 1990 (ref. 45). Pollution aerosol was modelled first as sulphates only[11], but new chemical measurements[46] show that downwind of the eastern United States[47] the contribution of carbonaceous material to AOT (30%) is double that of sulphates (16%), with water intake (48%) and black carbon (6%) accounting for the rest. Black carbon describes the effective fraction of elemental carbon that accounts for the absorption properties of the aerosol. Emission of black carbon is lower for newer engine technology so that black carbon contributes generally more to AOT in south and east Asia and Central America[32,33] (11%). Absorption by black carbon is not only related to its concentration, but also depends on its location in the aerosol particle — absorption can be two to three times stronger if the black carbon is located inside the scattering particle[48–51].

Smoke from vegetation fires

Smoke from vegetation fires is dominated by fine organic particles with varying concentrations of light-absorbing black carbon (regions b and d in Fig. 1a) emitted in the hot, flaming stage of the fire. In forest fires the flaming stage is followed by a long, cooler smouldering stage in which the thicker wood, not completely consumed, emits smoke (composed of organic particles without black carbon) in much greater quantities than during the flaming stage. Conversely, thin African grasses burn quickly in strong flaming fires, emitting large quantities of black carbon, without a smouldering stage. On average, 12% of African smoke AOT is due to absorption by black

Table 1 **Climatology of ambient aerosol properties averaged on the atmospheric column**

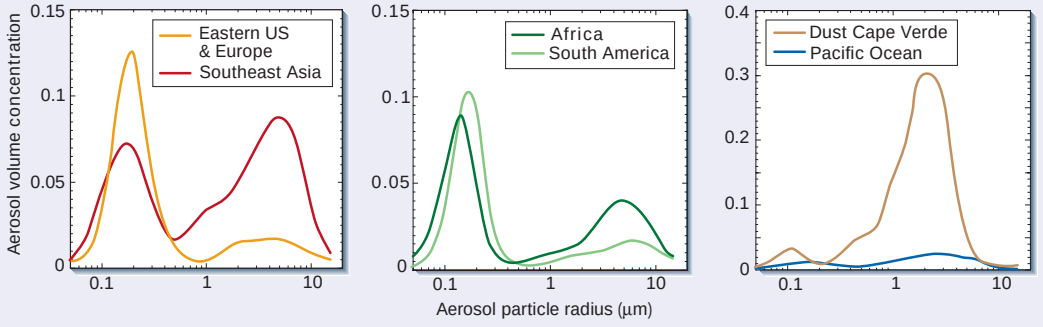

Analysis\Aerosol type	Regional pollution aerosol				Biomass burning			Dust	Oceanic
AERONET analysis	East. US	Europe	SE Asia	Cen. Am.	Boreal forest	Trop. forest	Savanna Africa–S.A.	Sahara–Saudi Arabia	Pacific Ocean
Time of the year	Jun–Sep		Jan–Apl	Jan–Dec		Jun–Nov		Jan–Dec	Jan–Dec
Average AOT	0.20		0.20	0.30	0.25–0.45		0.25–0.5	0.2–0.4	0.06
AOT_f	94%		95%	90%	95%		92%	25%	67%
% absorption of AOT	3%	6%	12%		7%		12%	5%	2%
MODIS analysis	North Atlantic 60–105° W 20–45° N		SE Asia 70–140° E 5–40° N		South Africa 15° W–30° E 0–20° S			West Africa 15–50° W 10–25° N	
Average AOT	0.18		0.24		0.31			0.30	
AOT_f	41%		44%		66%			33%	
ΔF_{TOA} (W m^{-2})	–8		–10		–10			–17	
ΔF_{SUR} (W m^{-2})	–10		–23		–30			–23	

The aerosol properties presented are based on two types of analysis. The top part of the table shows systematic multi-year measurements by the Aerosol Robotic Network (AERONET)[33,41] and *in situ* measurements[47,87,88], whereas data in the bottom part of the table are based on analysis of Moderate-resolution Imaging Spectroradiometer (MODIS) satellite data for September 2000. In the AERONET analysis, aerosol optical thickness (AOT) is a measure of the aerosol column concentration and is given at a wavelength of 0.55 μm. Four aerosol types are shown with a representative size distribution (in units of μm^3 per μm^2): (1) pollution from eastern United States (Greenbelt, Maryland) and Europe (Venice and Paris), southeast Asia (Maldives-INDOEX) and Central America (Mexico City); (2) biomass burning from Africa and South America; (3) dust over the Atlantic Ocean (Cape Verde); and (4) maritime aerosol over the Pacific Ocean (Lanai). The uncertainty in AOT is ±0.01; contribution of the fine mode to AOT (AOT_f) is given over the land with uncertainty of ±2%. In the MODIS data the uncertainty in AOT ranges from ±0.03 to ±0.06. The reflection of sunlight to space (ΔF_{TOA}) and reduction of surface illumination (ΔF_{SUR}) are based on the AERONET and MODIS data, using the radiative transfer code of Chou[89].

carbon[52], in contrast to 5% for Boreal fires[33]. Smoke is less hygroscopic than regional pollution aerosol, with only 10–20% of smoke AOT being associated with water for typical relative humidities of 80–85% in South America and Africa[53], compared with 50% for regional pollution aerosol[1]. Dense smoke plumes are found annually downwind of fires in South America (August–October), Central America (April and May), Southern Africa (July–September) and Central Africa (January–March)[5,6,54].

Dust

Dust is emitted from dry lakebeds in the Sahara, east Asia and the Saudi Arabian deserts[5,6] (regions a and c in Fig. 1b) that were flooded

Box 1
How do satellites observe aerosols?

Radiant energy reflected and emitted by the Earth carries with it a signature of the atmospheric and surface properties. By measuring the wavelength, angular and polarization properties of this energy, satellite sensors can quantify several atmospheric and surface properties. (Polarization is the degree of organization of the electric field of the scattered solar radiation into a given direction.)

The human eye is sensitive to a narrow spectral range of the solar spectrum, with spectral receptors for blue, green and red light. Depth perception is provided by our eyes having slightly different angles of observation. By analogy, aerosol remote sensing — for example, AVHRR (Advanced Very High Resolution Radiometer), METEOSAT and GOES (Geostationary Operational Environmental Satellite) — developed from using a single wavelength[5,91] and single angle of observation, like a colour-blind person with one eye. The TOMS instruments (for Total Ozone Mapping Spectrometer), flown since 1978, have two channels sensitive to ultraviolet light that were discovered to be excellent for observations[92,93] of elevated smoke or dust layers above scattering atmosphere (Box Fig. 1).

The first instrument designed for aerosol measurements, POLDER (Polarization and Directionality of the Earth's Reflectances)[26,38,40], uses a combination of spectral channels in a range wider than that of human vision (0.44–0.86 μm). The instrument comprises a wide-angle camera that observes the same target on the Earth at several different angles, up to zenith angle of 65°. POLDER also measures light polarization to detect fine aerosols over the land, taking advantage of the difference between the spectrally neutral polarized light reflected from the Earth's surface and the spectrally decreasing polarized light reflected by fine aerosols (see Fig. 4).

Two instruments, MODIS (Moderate-resolution Imaging Spectroradiometer) and MISR (Multi-angle Imaging Spectroradiometer), on the Terra satellite measure global aerosol concentrations and properties since 2000. Over the ocean, MODIS uses the aerosol spectral signature in a wide range (0.47–2.1 μm) to distinguish small pollution particles from coarse sea-salt and dust[25] (Box Fig. 2). MODIS measures aerosol optical thickness (AOT) with an estimated error of $\pm 0.05 \pm 0.20$AOT over the land[94] and $\pm 0.03 \pm 0.05$AOT over the ocean[95] (note that 0.03 is an offset due to uncertainty in the ocean state and 0.05AOT is due to uncertainty in aerosol properties). Over land, MODIS uses the 2.1-μm channel to observe surface-cover properties, estimate surface reflectance at visible wavelengths, and derive AOT[96] from the residual reflectance at the top of the atmosphere.

The amount of light escaping the top of the atmosphere is affected by the angle at which the light was reflected by the surface or atmosphere. MISR[27] takes advantage of this fact by detecting the reflected light at different viewing angles (nadir to 70° forward and backward) along the satellite's track in a narrower spectral range (0.44–0.86 μm). It is thus able to separate the aerosol signal from that of surface reflectance, and determine the aerosol properties. A mixed approach using two viewing directions but a wider spectral range (0.55–1.65 μm) is used by ATSR (Along Track Scanning Radiometer)[28] to derive the aerosol concentration and type.

Over bright desert the magnitude of dust absorption determines if dust brightens or darkens the image[82,97], and this property is used for its estimation. Such satellite measurements, in agreement with *in situ*[8], aircraft[98] and radiation-network[33] measurements of dust absorption, helped resolve a long-standing uncertainty in desert-dust absorption of sunlight[56].

The realization that aerosols affect surface temperature and precipitation patterns creates a demand for more informative spaceborne observations. We foresee several improvements in this respect. First, spaceborne instruments are being considered that combine a wide spectral and viewing-angle range[99] with polarization. Such instruments are expected to improve derivation of fine and coarse aerosols, including their sizes and refractive index (refractive index, an optical property, is sensitive to the aerosol composition and water intake[100]). Second, derivation of aerosol absorption over the oceans will be achieved by measuring the aerosol spectral attenuation of the bright glint.

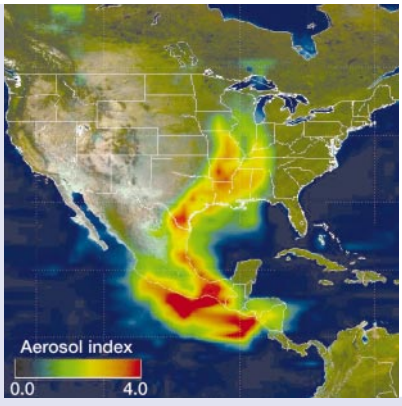

Box Figure 1 TOMS image showing heavy smoke aerosol transported to North America from large wild fires in Mexico on 15 May 1998. (Image courtesy of J. Herman, NASA/GSFC; see http://toms.gsfc.nasa.gov/aerosols/aerosols.html for additional images.)

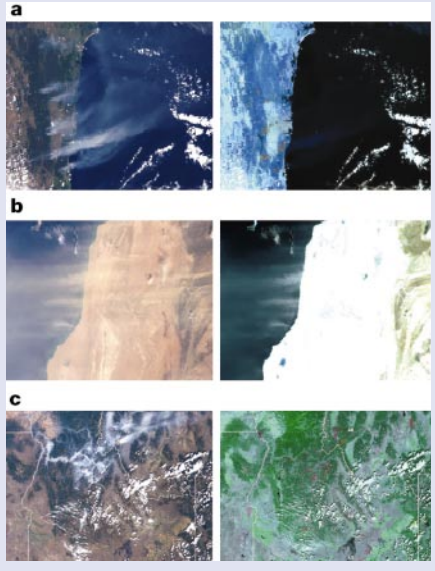

Box Figure 2 Spectral aerosol reflectance measured by MODIS. Panels in the left column show colour composites of channels in the visible spectrum and those on the right show composites in the near infrared spectrum. **a**, Fine smoke particles from fires in Australia (25 December 2001), which are invisible over the ocean in the near infrared[24]. **b**, Coarse dust particles emitted from West Africa (7 January 2002), which are visible in both panels over the ocean. **c**, Smoke in Idaho and Montana invisible in the mid-infrared over the land. The spectral measurements are used to detect smoke over land[31,95,96] and distinguish smoke from dust over the ocean.

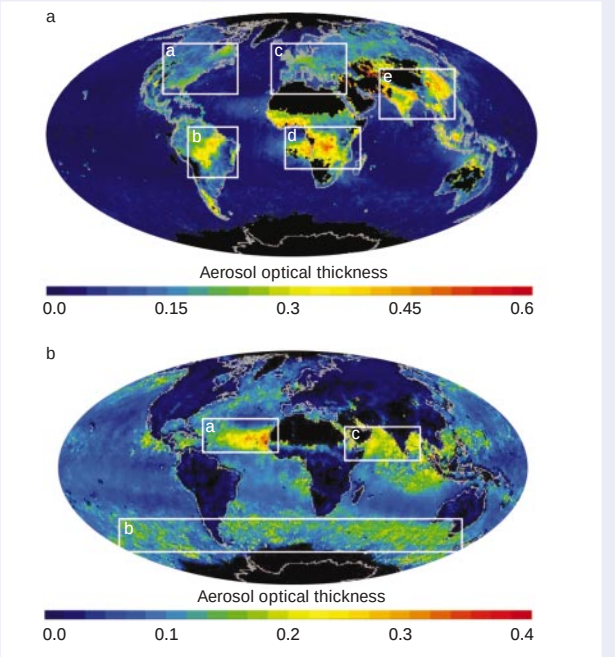

Figure 1 Global distribution of fine and coarse aerosol optical thickness (AOT) derived from MODIS measurements on the NASA Terra spacecraft for September 2000. AOT is a measure of the aerosol column concentration and is represented by the colour scale at a wavelength of 0.55 μm. Black regions have surface properties inappropriate for MODIS aerosol retrievals or very low solar elevations. The white boxes indicate regions with high aerosol concentrations. **a**, Distribution of fine AOT. The image shows fine particles in pollution from North America and Europe (regions a and c), vegetation fires in South America and southern Africa (regions b and d) and pollution in south and east Asia (region e). **b**, Distribution of coarse AOT. Coarse dust from Africa (region a), salt particles in the windy Southern Hemisphere (region b) and desert dust (region c).

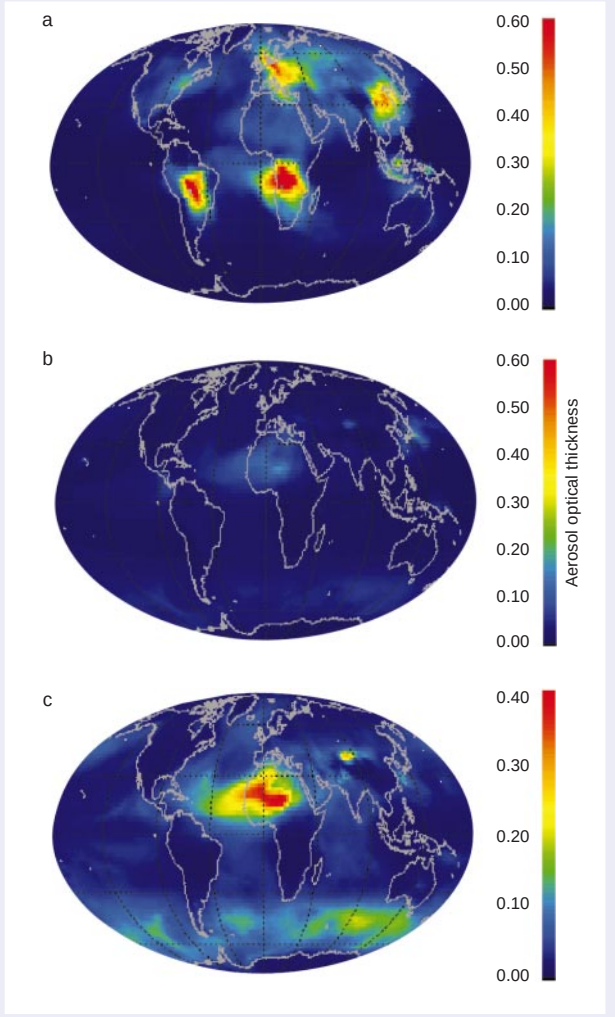

Figure 2 Model results of Chin *et al.*[23] that correspond to the MODIS data of September 2000. **a**, Anthropogenic fine aerosols; **b**, natural fine aerosols; and **c**, coarse aerosols composed of natural dust and salt.

in the Pleistocene era[55]. Almost no dust is observed from Australia[5], where the topography is mostly flat, because the arid regions are old and highly weathered[55]. An unknown amount of dust is emitted from disturbed soils in Africa and east Asia. A previous estimate that 30–50% (ref. 56) of African dust results from human impact is questioned by new satellite observations using the ultraviolet part of the solar spectrum[6] (Box 1); these show that African dust originates mostly from uninhabited regions north of 15° N (ref. 55). Dust emission from Africa is influenced by large-scale air circulation[57], which affects flow from the continent, and drought conditions. The highest dust production matches drought conditions in the strongest El Niño year of 1983 (ref. 7).

Dust AOT is dominated by coarse particles[58] with varying concentrations of iron oxide (rust) that absorbs light in the blue and ultraviolet wavelengths. However, African dust transported to Florida contains high concentrations of fine particles (10–100 $\mu g\ m^{-3}$) during the summer months and exceeds local pollution standards on particulate matter[42]. Dust from east Asia, from both natural sources and land use, is elevated to a height of 3–5 km with a pollution layer under it at 0–2 km (ref. 59), and is transported during April and May to North America. In April 2001 such a dust storm generated hazy conditions (AOT of 0.4) as far away as Boulder, Colorado (G. Feingold personal communication). On its way to North America, dust deposited in the Atlantic and Pacific Oceans provides key nutrients such as iron to oceanic phytoplankton[60].

Oceanic aerosol

Oceanic aerosol is shown in the blue regions of Fig. 1b and the elevated green values at latitudes south of 40° S (region b in Fig. 1b). It is composed of coarse salt particles emitted from bursting sea foam in windy conditions and fine sulphate particles from oceanic emissions[61]. Oceanic aerosol generally absorbs very little sunlight[33,62] — its AOT is estimated to average 0.07 in most regions[32,62], but increases in the windy region south of 40° S to 0.2 (ref. 23).

Anthropogenic component

It is difficult to distinguish anthropogenic from natural aerosols as even individual particles can have both natural and anthropogenic components[30,32,63]. Precise description of aerosol composition requires *in situ* chemical measurements that are restricted in time and location. However, it is possible to estimate the anthropogenic part of aerosols using a combination of satellite data, aerosol models[23,24,44] and information on urban and agricultural activities and fire practices. For example, in Fig. 1 we see that anthropogenic aerosols downwind from vegetation fires and regions of industrial pollution are characterized by high concentration of fine particles. Aerosol models[23] confirm this finding, and further show that natural fine aerosols emitted from large-area oceanic and land sources exhibit much smaller spatial variability (Fig. 2). An example of daily satellite data and model calculations (Fig. 3) shows clear distinction between dust plume (coarse particles) and the regional pollution (fine particles). The model simulations confirm this distinction.

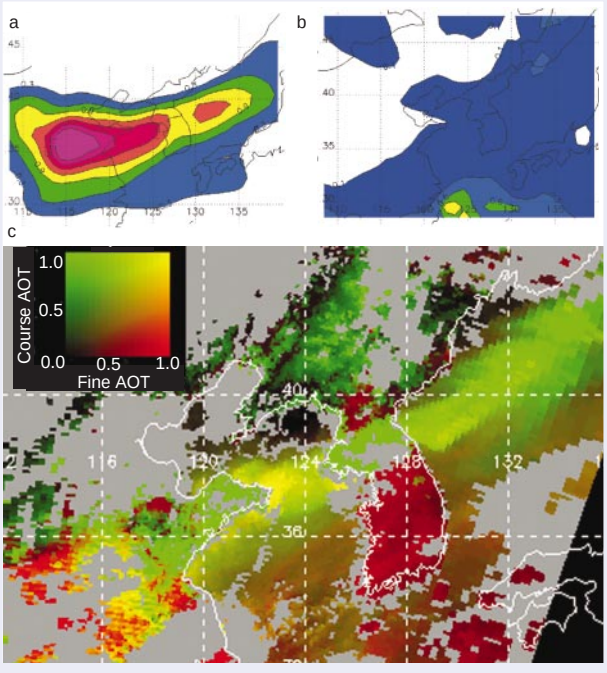

Figure 3 Satellite data and model calculations for a dust episode in east Asia advected over a pollution layer on 20 March 2001. **a**, **b**, NAAPS aerosol model simulation[90] of the optical thickness of the coarse dust particles (**a**) and the fine sulphate particles (**b**); the optical thickness varies from 0.3 for the blue to 1.5 for the red. **c**, Optical thickness of fine particles (red) associated with air pollution and the coarse dust (green) derived from the MODIS data on the Terra satellite.

An example of the relationship between population density and pollution concentration is shown in Fig. 4. Proximity of dust to desert or agricultural area can be used as an indicator for natural desert dust. Continued improvements in the models, constrained by new, detailed global measurements, will enable us to isolate the anthropogenic aerosol component.

In the Indian Ocean Experiment, chemical separation of aerosols into natural and anthropogenic components[32] shows that the natural aerosol AOT is 0.07, with an additional 0.2–0.6 over the Bay of Bengal resulting from anthropogenic activity[64]. But pinpointing the anthropogenic source is proving difficult. Aerosol chemical composition can be used as a 'fingerprint' of the source, and a ratio of 1:2 between black carbon and total carbonaceous aerosol or sulphates suggests that the aerosol is emitted primarily from fossil fuel consumption[32]. But aerosol concentration varies through the year, whereas the relatively steady use of fossil fuel in the tropics, with its small variation of energy use from winter to summer[64], would suggest a stable aerosol concentration. A correlation between aerosol concentration and number of fires in India[64] suggests a large contribution of biomass burning. Analysis of aerosols and trace gases (CO and SO_2) suggests a mixed origin, both from fossil fuel and bio-fuel burning in the same proximity[65].

Aerosol direct forcing

The climate system varies naturally, through the dynamic interplay between atmospheric, oceanic and terrestrial moisture and energy. However, the radiative effects resulting from an increase in the concentration of anthropogenic aerosol or greenhouse gases, called radiative forcing, cause a net change in the Earth's absorbed and emitted solar and thermal energy and therefore are the basic ingredients of climate change[1].

A negative radiative forcing indicates that the Earth–atmosphere system loses radiant energy, resulting in cooling. Models of the climate system[1] show a direct relationship between radiative forcing and average global surface temperature, which rises 0.4–1.2 °C for every 1 W m^{-2} of forcing. However, this relationship may break down for strongly absorbing aerosols[12,14,15].

Dust and smoke serve as an example of weakly and strongly absorbing aerosols (see Table 1). Absorption accounts for 5% and 12% of AOT for Saharan Desert dust and for aerosols in south and east Asia, respectively[33]. In September 2000, dust reflected 17 W m^{-2} of sunlight to space, thus reducing by an equivalent amount the energy available to heat the Earth–atmosphere system. At the same time, the dust reduced surface illumination by 23 W m^{-2}; the difference (6 W m^{-2}) is due to the absorption of sunlight. The aerosols in south and east Asia also reduced surface illumination by 23 W m^{-2}, but absorbed 13 W m^{-2}, reflecting only 10 W m^{-2} to space[32]. Figure 5 shows the large regional extent of the aerosol radiative effects for these two aerosol types.

Another example of the radiative effects of weakly or strongly absorbing aerosol occurs over the Atlantic Ocean. Absorbing smoke is transported from Africa across the Southern Atlantic and less absorbing pollution aerosol is transported from North America in the Northern Atlantic (Fig. 1). In September 2000, aerosols found in these two

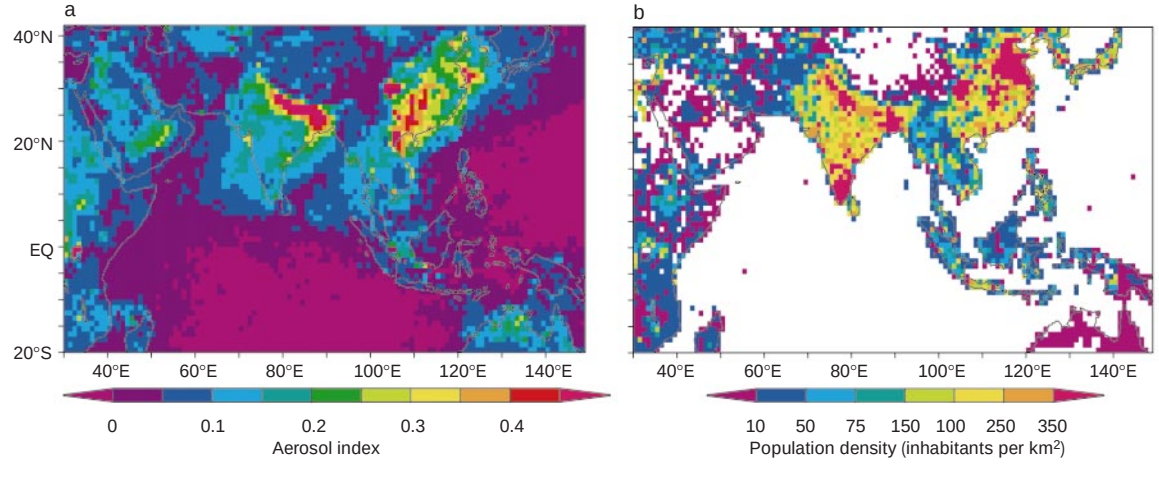

Figure 4 Comparison between concentration of anthropogenic aerosol and population density. **a**, Aerosol polarization index derived from the data of the POLDER instrument flown on ADEOS-1 in February 1997. The index is derived from measurements of polarization of scattered solar light and is sensitive only to the presence of fine aerosol particles that in high concentration originate from anthropogenic sources. **b**, Population density map (inhabitants per square kilometre).

regions reflected 10 and 8 W m^{-2}, respectively, of sunlight to space. But the impact on surface illumination is three times larger for the smoke than for the pollution aerosol (30 W m^{-2} versus 10 W m^{-2}). Model calculations show that such strong aerosol absorption occurring in the lower troposphere heats the air layer, reducing its relative humidity and temperature gradients[32], and increasing atmospheric stability. This decreases cloudiness[15] and possibly reduces or prevents precipitation[20] that could have washed the aerosols from the atmosphere.

The results in Fig. 5 and Table 1 were computed for cloud-free oceanic regions. In cloudy conditions, the aerosol radiative effect depends on the fraction of absorbing aerosol located above clouds[14], where the particles can absorb up to three times more sunlight than aerosol in cloud-free conditions[66]. Absorbing aerosols may even have a positive (warming) rather than negative (cooling) radiative impact. Over dark oceans (albedo of 6%) the aerosol absorption has to be as high as 15% of AOT to result in warming, but 10% is enough over the brighter land (albedo of 20%), and only 5% if the aerosol layer is above boundary-layer clouds[14].

Knowledge of the vertical distribution of aerosols and clouds is therefore needed to calculate the impact of aerosol radiative effects. Elevated aerosol plumes occur during long-range transport of aerosols. For example, smoke from forest fires in Canada was found over Greece at 2–3 km altitude[67], above the local boundary-layer clouds; Saharan dust is transported over Europe at 3–10 km elevation[68]; and smoke intrusions from fires in Mexico[69] and northeast Canada are transported across North America at altitudes of 3–5 km. With the launch of space lidars[70] in the next few years we will begin to make the global measurements of the aerosol and cloud profiles needed to assess aerosol radiative forcing.

Aerosol modification of clouds and precipitation

Each cloud drop requires an aerosol particle to condense upon; clouds could not form otherwise. Thus the concentration, size and composition of the aerosols that can act as cloud condensation nuclei (CCN) determine the cloud properties[9,17,18], evolution and development of precipitation[20]. However, availability of moisture, updrafts and cloud formation are influenced mainly by large-scale dynamic processes. Although natural aerosols are needed to form clouds, it seems that urban haze and smoke aerosols take every opportunity to reduce formation of precipitation and affect cloud radiative properties at the same time (Fig. 6).

Cloud base

Aircraft measurements show that in polluted air a sixfold increase in the number of fine aerosols per unit volume of air produces a three- to fivefold increase in the droplet concentration[2,71]. Analysis of global satellite data shows that such a change in aerosol concentration corresponds to 10–25% smaller cloud droplets[17,38] (Fig. 7), because the condensed water is divided into more numerous droplets. Clouds with smaller, more numerous droplets have a larger surface area and a corresponding increase in reflectivity of up to 30% (ref. 17). This increase in the reflection of sunlight to space, called the first aerosol indirect effect, was proposed by Twomey, based on two decades of aircraft sampling, to possibly rival the greenhouse forcing[9]. If these global cloud modifications can be attributed to anthropogenic effects[72], they would translate into a solar radiative forcing of –0.5 to –1.5 W m^{-2} (refs 17, 73).

The actual effect of aerosols on cloud droplets, as inferred from global measurements from aircraft[2] and satellites[17,38], is 1.5–3 times smaller than that expected by Twomey for constant liquid water content[9]. In polluted air, above a given threshold of CCN concentration, the concentration of cloud droplets does not increase further; this results from competition between the more numerous CCN for water vapour[2], and it may explain the smaller global effect. The threshold depends on cloud dynamics, availability of moisture, aerosol size distribution and chemical properties. The larger and more hygroscopic the particles, the greater their ability to

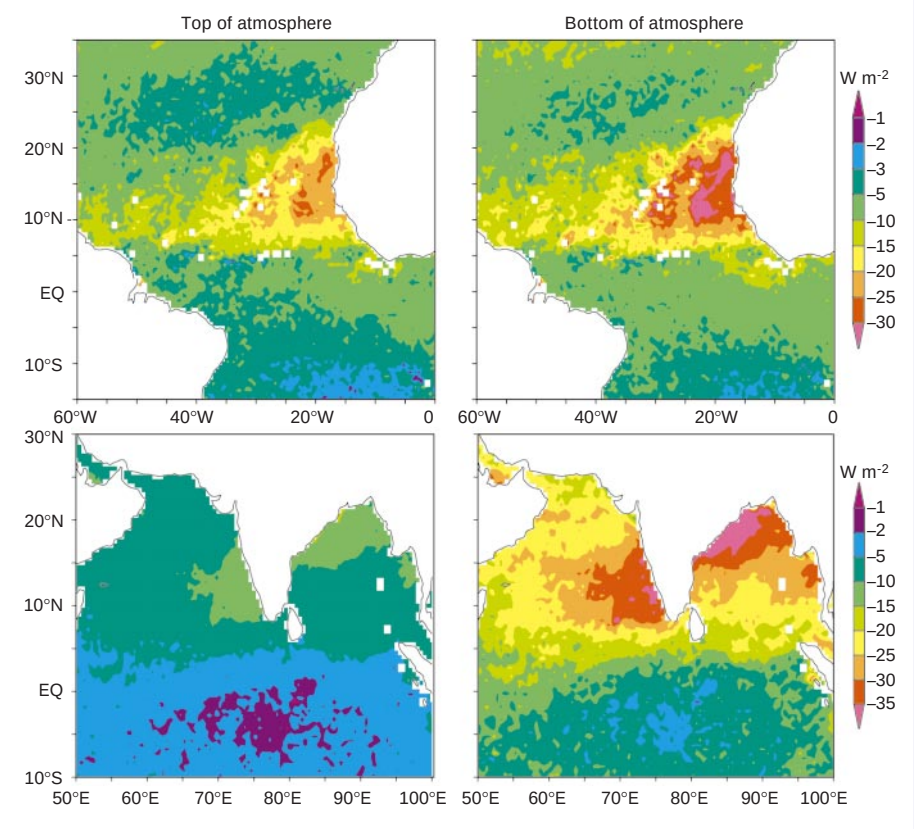

Figure 5 Solar radiative perturbation at the top of the atmosphere and the surface for the tropical Atlantic and Indian Ocean. Top of the atmosphere (left parts) and surface (right parts) solar radiative perturbation (W m^{-2}) in clear sky is shown for the tropical Atlantic Ocean in May 1997 (upper parts) and the Indian Ocean in March 1997 (lower parts). The radiative perturbation is derived from the POLDER daily analysis of the aerosol optical depth combined with aerosol models modified to reproduce the aerosol absorption of Table 1. Over the Indian Ocean the perturbation is three times larger at the surface than at the top of atmosphere, as the aerosol-absorbed sunlight does not reach the surface.

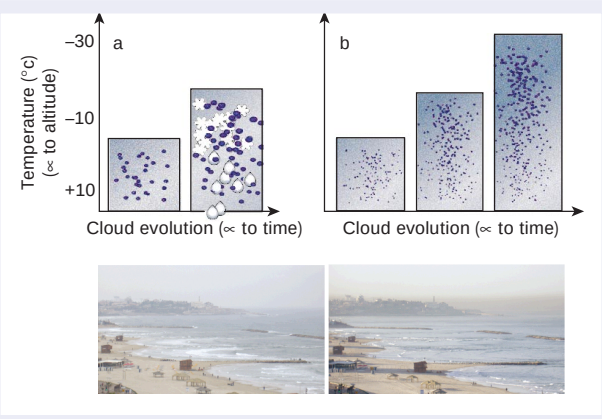

Figure 6 Schematic diagram of cloud formation in a clean and polluted atmosphere. **a**, In a clean atmosphere, the cloud droplet size increases with cloud development until liquid precipitation or glaciation and precipitation take place. **b**, In polluted clouds, the availability of cloud condensation nuclei decreases cloud droplet development. In clouds with strong updrafts the developed cloud can be supercooled with no glaciation down to –37.5 °C. The filled circles show the location of droplets of varying size, the asterisks show the location of ice crystals, and the oval shapes indicate rain drops.

compete at a given cloud updraft speed[74]. The presence of even a few supermicron CCN particles per litre, such as sea salt or dust particles coated with sulphates[63], may reduce the indirect effect of pollution aerosol and produce precipitation[75].

Additional aerosol processes have to be considered, such as the possibility that water-soluble organic compounds present in the particle and the presence of soluble gases (HNO_3) in the atmosphere help the aerosols to take up water vapour and further increase the concentration of cloud droplets and the indirect forcing[76]. A contrary effect can take place from organic films that retard droplet growth and reduce drop concentration[77].

Cloud development

In clean conditions the cloud droplet size increases as the cloud develops and extends in the vertical direction until the droplet reaches a critical radius of ~15 μm (ref. 36) for the onset of liquid precipitation. Alternatively, the droplet may freeze if the cloud top temperature reaches –10 °C. In pollution plumes over Australia and Canada, and smoke plumes over Indonesia, satellite data show not only smaller droplets at the cloud base (5–8 μm radius compared with 10–15 μm in clean conditions), but also a lack of increase in droplet size as the cloud develops, rising through the atmosphere and accumulating water vapour. Consequently, precipitation does not occur or is delayed in polluted water clouds[20,21]. In the same regions, non-polluted cloud droplets grow to 20–30 μm and precipitation occurs. This suppression of precipitation was also observed for stratiform clouds polluted by emissions from ship stacks[36] and for polluted cumulus clouds in the Indian Ocean[71].

The high concentration of aerosol supplies new CCN to condense the excess water vapour as the cloud cools down. The result is an increase in the cloud liquid water content, cloud lifetime and area of coverage — called the second aerosol indirect effect. The global importance of this effect is still not clear. Analysis of changes in cloud fraction and precipitation throughout the last century suggests that more clouds are needed for the same amount of precipitation, as would be expected given the inhibitory effect of pollution on precipitation (D. Rosenfeld personal communication, from data in ref. 1).

Ice crystals

Water clouds that cannot precipitate owing to the high concentration of aerosols could still precipitate once the droplets freeze.

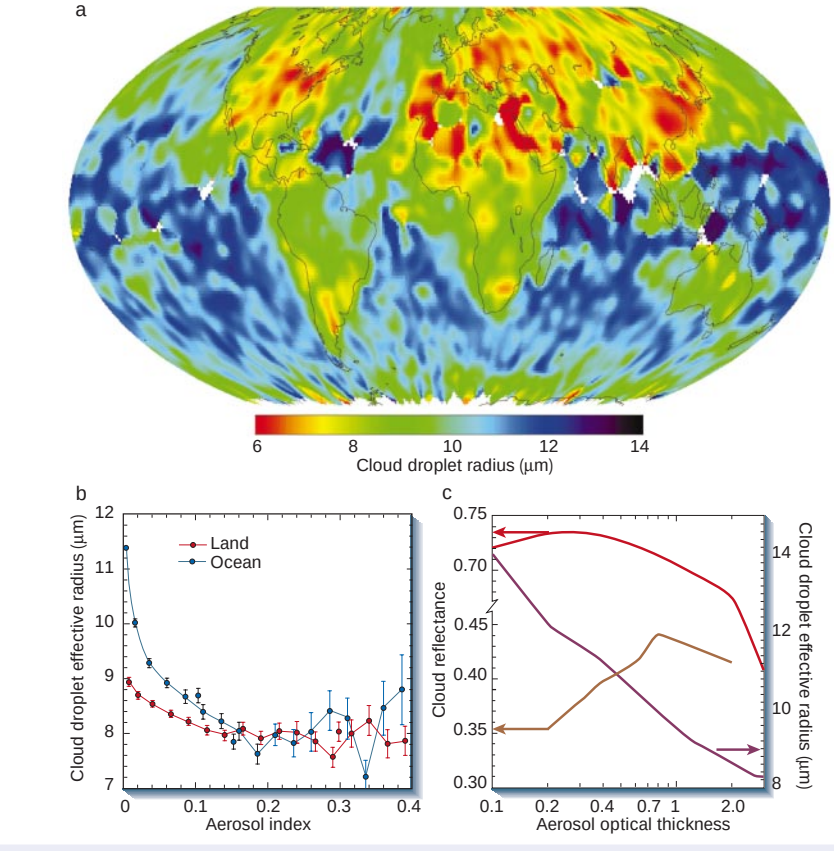

Figure 7 Effect of aerosol on cloud droplet and reflectance derived from POLDER and AVHRR spaceborne measurements. **a**, Seasonal (March–May 1997) average droplet size in liquid water clouds estimated from the POLDER measurements[31]. **b**, The dependence of the droplet size on the aerosol index, also derived from POLDER over land (red) and ocean (blue). **c**, Analysis of AVHRR data for the dependence of the droplet size (purple) and cloud reflectance (brown and red) on aerosol optical thickness over the Amazon Basin during the dry burning season of 1987 (refs 16, 19). The reflectance of low-level clouds (brown) with reflectance of 0.35 increases with the aerosol concentration and the reflectance of bright clouds (red) decreases.

However, measurements in a deep convective cloud with a strong updraft show that the freezing process is postponed until the cloud reaches temperatures of –37.5 °C. Strong updrafts and condensation lead to a high concentration of small cloud droplets. These droplets do not collide efficiently to form raindrops, nor do they freeze at –10 °C. The result is a supercooled water cloud, thus eliminating an alternative way for clouds to precipitate[78]. Model simulations suggest that this process requires the presence of high CCN concentrations (1,260 cm^{-3}) and vigorous updrafts[79].

Cloud formation

The presence of light-absorbing black carbon in aerosols can also affect cloud properties. Models show that heating of the lower troposphere by aerosol absorption reduces cloud formation[15], an effect referred to as the semi-direct effect[14]. There are no direct measurements of this effect, but analysis of satellite data of clouds embedded in varying concentrations of smoke from fires in the Amazon basin[19] shows that for the thicker clouds an increase in the smoke AOT from 0.2 to 3 raises the cloud-top temperature by 4 °C, decreases the cloud reflectance by 0.13, while still reducing the droplet size by 40% (Fig. 7c). The simultaneous rise in the cloud-top temperature and reduction in reflectance — more than black carbon absorption itself can explain[19] — indicates the possibility of a reduction in convection, thereby causing a decrease in the updraft speed and in the amount of liquid water available to form the cloud[19].

The effect of aerosols on cloud droplet size is better understood than their effect on precipitation. Additional studies are needed to quantify the indirect effect of aerosols on climate, but the potential for a significant cooling in most regions is indicated. The reduction of the precipitation efficiency by anthropogenic aerosols has the potential to shift precipitation away from polluted regions[34]. Because the continents are more polluted than the ocean, this can cause a loss of fresh water over the continents, and in particular around populated regions. However, long-term regional studies that can measure the significance of this effect are still not available.

Aerosols in climate change

The cooling influence of aerosols on climate, directly through the reflection of sunlight to space[10] and indirectly through changes in cloud properties[9], has been appreciated for over a decade, and has triggered a large number of observations, simulations and analyses. The effect of anthropogenic aerosols is not limited to cooling by sulphates. Instead, carbonaceous compounds that include light-absorbing black carbon can be an important warming agent, and the sign of the temperature change from aerosols[80] can vary depending on the aerosols' radiative properties[81,82] and their distribution over the dark ocean and reflective land. The cooling of the Earth's surface from absorbing aerosols (compared with the top of the atmosphere) and consequential warming of the atmosphere causes a flattened vertical temperature profile in the troposphere, which is expected to slow the hydrologic cycle[2], reduce evaporation from the surface and reduce cloud formation[14,15]. It has also been suggested that as aerosols tend to reduce cloud droplet sizes[17,38], and hence precipitation[20], rain and snow may be shifted from highly polluted populated areas to the more pristine oceanic regions[34]. This raises the question of whether there has been or will be a change in the availability of fresh water due to aerosols.

Future research will need to unravel the magnitude of the aerosol effect on clouds and precipitation, on regional and global scales, and its sensitivity to aerosol chemistry and cloud dynamics. Given the importance of the absorption of sunlight by black carbon[12], a quantitative assessment of black carbon sources[83], its lifetime in the atmosphere, its distribution around the globe[54] and its impact on the hydrologic cycle[2] will need to be explored.

To associate the aerosol impact with human activity, we need to distinguish natural from anthropogenic aerosols. By measuring separately fine and coarse particles, remote sensors distinguish the emission and transport of dust (mostly from natural sources) from pollution and smoke aerosols (mostly anthropogenic) around the planet. Remote sensors also map the distribution and properties of clouds[17,24,38,72], precipitation[20,21] and the Earth's reflected solar and emitted thermal energy to space[39,84,85], as these atmospheric constituents are impacted by the aerosol. These global data and source characterization[83] feed aerosol models[11,23,86] to show us an increasingly realistic picture of aerosols around the world and their impact on the environment. To achieve these ends, ground-based and *in situ* measurements, models and satellite observation have to be each improved and integrated. □

doi:10.1038/nature01091

1. Intergovernmental Panel on Climate Change. *Climate Change 2001—The Scientific Basis* (contribution of working group I to the Third Assessment Report of the Intergovernmental Panel on Climate Change) (Cambridge Univ. Press, Cambridge, 2001).
2. Ramanathan, V. *et al.* Aerosols, climate, and the hydrological cycle. *Science* **294,** 2119–2124 (2001).
3. Andreae, M. O. *et al.* External mixture of sea salt, silicates, and excess sulfate in marine aerosols. *Science* **232,** 1620–1623 (1986).
4. Keeling, C. D. The concentration and isotopic abundances of carbon dioxide in the atmosphere. *Tellus* **12,** 200–203 (1960).
5. Husar, R. B., Prospero, J. & Stowe, L. L. Characterization of tropospheric aerosols over the oceans with the NOAA AVHRR optical thickness operational product. *J. Geophys. Res.* **102,** 16889–16909 (1997).
6. Herman, J. R. *et al.* Global distribution of UV-absorbing aerosol from Nimbus-7/TOMS data. *J. Geophys. Res.* **102,** 16911–16922 (1997).
7. Prospero, J. M. & Nees, R. T. Impact of the North African drought and El Niño on mineral dust in the Barbados trade wind. *Nature* **320,** 735–738 (1986).
8. Clarke, A. D. & Charlson, R. J. Radiative properties of the background aerosol: absorption component of extinction. *Science* **229,** 263–265 (1985).
9. Twomey, S. A., Piepgrass, M. & Wolfe, T. L. An assessment of the impact of pollution on the global albedo. *Tellus* **36B,** 356–366 (1984).
10. Charlson, R. J. *et al.* Climate forcing of anthropogenic aerosols. *Science* **255,** 423–430 (1992).
11. Kiehl, J. T. & Briegleb, B. P. The relative roles of sulfate aerosols and greenhouse gases in climate forcing. *Science* **260,** 311–314 (1993).
12. Satheesh, S. K. & Ramanathan, V. Large differences in tropical aerosol forcing at the top of the atmosphere and Earth's surface. *Nature* **405,** 60–63 (2000).
13. Eck, T. F. *et al.* Measurements of irradiance attenuation and estimation of the aerosol single scattering albedo for biomass burning in Amazonia. *J. Geophys. Res.* **103,** 31865–31878 (1998).
14. Hansen, J., Sato, M. & Ruedy, R. Radiative forcing and climate response. *J. Geophys. Res.* **102,** 6831–6864 (1997).
15. Ackerman, A. S. *et al.* Reduction of tropical cloudiness by soot. *Science* **288,** 1042–1047 (2000).
16. Kaufman, Y. J. & Fraser, R. S. Confirmation of the smoke particles effect on clouds and climate. *Science* **277,** 1636–1639 (1997).
17. Nakajima, T. *et al.* A possible correlation between satellite-derived cloud and aerosol microphysical parameters. *Geophys. Res. Lett.* **28,** 1171–1174 (2001).
18. Coakley, J. A. Jr, Bernstein, R. L. & Durkee, P. A. Effect of ship stack effluents on cloud reflectance. *Science* **237,** 953–956 (1987).
19. Kaufman, Y. J. & Nakajima, T. Effect of Amazon smoke on cloud microphysics and albedo. *J. Appl. Meteorol.* **32,** 729–744 (1993).
20. Rosenfeld, D. TRMM observed first direct evidence of smoke from forest fires inhibiting rainfall. *Geophys. Res. Lett.* **26,** 3105–3108 (1999).
21. Rosenfeld, D. Suppression of rain and snow by urban and industrial air pollution. *Science* **287,** 1793–1796 (2000).
22. Boucher, O. & Haywood, J. On summing the components of radiative forcing of climate change. *Clim. Dynam.* **18,** 297–302 (2001).
23. Chin, M *et al.* Tropospheric aerosol optical thickness from the GOCART model and comparisons with satellite and Sun photometer measurements. *J. Atmos. Sci.* **59,** 461–483 (2002).
24. King, M. D. *et al.* Remote sensing of tropospheric aerosols from space: past, present and future. *Bull. Am. Meteorol. Soc.* **80,** 2229–2259 (1999).
25. Tanré, D. *et al.* Remote sensing of aerosol over oceans from EOS-MODIS. *J. Geophys. Res.* **102,** 16971–16988 (1997).
26. Deuzé, J.-L. *et al.* Estimate of the aerosol properties over the ocean with POLDER. *J. Geophys. Res.* **105,** 15329–15346 (2000).
27. Diner, D. J. *et al.* MISR aerosol optical depth retrievals over southern Africa during the SAFARI-2000 dry season campaign. *Geophys. Res. Lett.* **28,** 3127–3130 (2001).
28. Veefkind, J. P., de Leeuw, G. & Durkee, P. A. Retrieval of aerosol optical depth over land using two-angle view satellite radiometry during TARFOX. *Geophys. Res. Lett.* **25,** 3135–3138 (1998).
29. Delene, D. J. & Ogren, J. A. Variability of aerosol optical properties at four North American surface monitoring sites. *J. Atmos. Sci.* **59,** 1135–1150 (2002).
30. Artaxo, P. *et al.* Large scale aerosol source apportionment in Amazonia. *J. Geophys. Res.* **103,** 31837–31847 (1998).
31. Kaufman, Y. J. *et al.* The Smoke, Clouds and Radiation experiment in Brazil (SCAR-B). *J. Geophys. Res.* **103,** 31783–31808 (1998).
32. Ramanathan, V. *et al.* The Indian Ocean Experiment: an integrated analysis of the climate forcing and effects of the great Indo-Asian haze. *J. Geophys. Res.* **106,** 28371–28398 (2001).
33. Dubovik, O. *et al.* Variability of absorption and optical properties of key aerosol types observed in worldwide locations. *J. Atmos. Sci.* **59,** 590–608 (2002).
34. Rotstayn, L. D., Ryan, B. F. & Penner, J. E. Precipitation changes in a GCM resulting from the indirect effects of anthropogenic aerosols. *Geophys. Res. Lett.* **27,** 3045–3048 (2000).
35. Lohmann, U. & Feichter, J. Impact of sulfate aerosols on albedo and lifetime of clouds: a sensitivity study with the ECHAM4 GCM. *J. Geophys. Res. Atmos.* **102,** 13685–13700 (1997).

36. Albrecht B. A. Aerosols, cloud microphysics, and fractional cloudiness. *Science* **245,** 1227–1230 (1989).
37. Penner, J. E., Dickinson, R. E. & O'Neill, C. A. Effects of aerosol from biomass burning on the global radiation budget. *Science* **256,** 1432–1433 (1992).
38. Bréon, F.-M., Tanré, D. & Generoso, S. Aerosol effect on cloud droplet size monitored from satellite. *Science* **295,** 834–838 (2002).
39. Wielicki, B. A. *et al.* Clouds and the earth's radiant energy system (CERES): an earth observing system experiment. *Bull. Am. Meteorol. Soc.* **77,** 853–868 (1996).
40. Herman, M. *et al.* Remote sensing of aerosol over land surfaces including polarization measurements and application to POLDER measurements. *J. Geophys. Res.* **102,** 17039–17049 (1997).
41. Holben, B. N. *et al.* An emerging ground based aerosol climatology: aerosol optical depth from AERONET. *J. Geophys. Res.* **106,** 12067–12097 (2001).
42. Prospero, J. M. Long term measurements of the transport of African mineral dust to the Southern US: implications for regional air quality. *J. Geophys. Res.* **104,** 15917–15927 (1999).
43. Bates T. S. *et al.* International Global Atmospheric Chemistry (IGAC) project's first aerosol characterization experiment ACE-1: overview. *J. Geophys. Res.* **103,** 16297–16318 (1998).
44. Takemura, T. *et al.* Single-scattering albedo and radiative forcing of various aerosol species with a global three-dimensional model. *J. Clim.* **15,** 333–352 (2002).
45. Luo Y. F. *et al.* Characteristics of the spatial distribution and yearly variation of aerosol optical depth over China in last 30 years. *J. Geophys. Res.* **106,** 14501–14513 (2001).
46. Novakov, T., Hegg, D. A. & Hobbs, P. V. Airborne measurements of carbonaceous aerosols on the East Coast of the United States. *J. Geophys. Res.* **102,** 30023–30030 (1997).
47. Hegg, D. A. *et al.* Chemical apportionment of aerosol column optical depth off the mid-Atlantic coast of the United States. *J. Geophys. Res.* **102,** 25293–25303 (1997).
48. Ackerman, T. P. & Toon, O. B. Absorption of visible radiation in atmosphere containing mixtures of absorbing and non-absorbing particles. *Appl. Opt.* **20,** 3661–3668 (1981).
49. Martins, J. V. *et al.* Effects of black carbon content, particle size, and mixing on light absorption by aerosol particles from biomass burning in Brazil. *J. Geophys. Res.* **103,** 32041–32050 (1998).
50. Haywood, J. & Boucher, O. Estimates of the direct and indirect radiative forcing due to tropospheric aerosols: a review. *Rev. Geophys.* **38,** 513–543 (2000).
51. Jacobson, M. Z. Strong radiative heating due to the mixing state of black carbon in atmospheric aerosols. *Nature* **409,** 695–697 (2001).
52. Eck, T. F. *et al.* Characterization of the optical properties of biomass burning aerosols in Zambia during the 1997 ZIBBEE field campaign. *J. Geophys. Res.* **106,** 3425–3448 (2001).
53. Ross, J. L., Hobbs, P. V. & Holben, B. Radiative characteristics of regional hazes dominated by smoke from biomass burning in Brazil: closure tests and direct radiative forcing. *J. Geophys. Res.* **103,** 31925–31941 (1998).
54. Liousse, C. *et al.* A Three-dimensional model study of carbonaceous aerosols. *J. Geophys. Res.* **101,** 19411–19432 (1996).
55. Prospero, J. M. *et al.* Environmental characterization of global sources of atmospheric soil dust identified with the NIMBUS-7 TOMS absorbing aerosol product. *Geophys. Rev.* (in the press).
56. Sokolik, I. N. & Toon, O. B. Direct radiative forcing by anthropogenic airborne mineral aerosol. *Nature* **381,** 681–683 (1996).
57. Moulin, C. *et al.* Control of atmospheric export of dust from North Africa by the North Atlantic oscillation. *Nature* **387,** 691–694 (1997).
58. Tanré, D. *et al.* Climatology of dust aerosol size distribution and optical properties derived from remotely sensed data in the solar spectrum. *J. Geophys. Res.* **106,** 18205–18218 (2001).
59. Clarke, A. D. & Kapustin, V. N. A Pacific aerosol survey, part 1: a decade of data on particle formation, transport, evolution, and mixing in the troposphere. *J. Atmos. Sci.* **59,** 363–382 (2002).
60. Gao, Y. *et al.* Seasonal distribution of Aeolian iron fluxes to the global ocean. *Geophys. Res. Lett.* **28,** 29–33 (2001).
61. Hoppel, W. A. *et al.* Aerosol size distribution and optical properties found in the marine boundary layer over the Atlantic Ocean. *J. Geophys. Res.* **95,** 3659–3686 (1990).
62. Smirnov, A. *et al.* Optical properties of atmospheric aerosol in maritime environments. *J. Atmos. Sci.* **59,** 501–523 (2002).
63. Levin, Z., Ganor, E. & Gladstein, V. The effects of desert particles coated with sulfate on rain formation in the Eastern Mediterranean. *J. Appl. Meteorol.* **35,** 1511–1523 (1996).
64. Leon, J. F. *et al.* Large-scale advection of continental aerosols during INDOEX. *J. Geophys. Res.* **106,** 28427–28439 (2001).
65. Reiner T. *et al.* Chemical characterization of pollution layers over the tropical Indian Ocean: signatures of emissions from biomass and fossil fuel burning. *J. Geophys. Res.* **106,** 28497–28510 (2001).
66. Liao, H. & Seinfeld, J. H. Effect of clouds on direct aerosol radiative forcing of climate. *J. Geophys. Res.* **103,** 3781–3788 (1998).
67. Formenti, P. *et al.* Aerosol optical properties and large-scale transport of air masses: observations at a coastal and a semiarid site in the eastern Mediterranean during summer 1998. *J. Geophys. Res.* **106,** 9807–9826 (2001).
68. Gobbi, G. P. *et al.* Altitude-resolved properties of a Saharan dust event over the Mediterranean. *Atmos. Environ.* **34,** 5119–5127 (2000).
69. Kreidenweis, S. M. *et al.* Smoke aerosol from biomass burning in Mexico: hygroscopic smoke optical model. *J. Geophys. Res.* **106,** 4831–4844 (2001).
70. Winker, D. M., Couch, R. H. & McCormick, M. P. An overview of LITE: NASA's lidar in-space technology experiment. *Proc. IEEE* **84,** 164–180 (1996).
71. Heymsfield A. J. & McFarquhar, G. M. Microphysics of INDOEX clean and polluted trade cumulus clouds. *J. Geophys. Res.* **106,** 28653–28674 (2001).
72. Han, Q., Rossow, W. B. & Lacis, A. A. Near global survey of effective droplet radii in liquid water clouds using ISCCP data. *J. Clim.* **7,** 465–496 (1994).
73. Boucher, O. GCM estimate of the indirect aerosol forcing using satellite-retrieved cloud droplet effective radii. *J. Clim.* **8,** 1403–1409 (1995).
74. Feingold, G. *et al.* Analysis of smoke impact on clouds in Brazilian biomass burning regions: an extension of Twomey's approach. *J. Geophys. Res.* **106,** 22907–22922 (2001).
75. Feingold, G. *et al.* The impact of giant cloud condensation nuclei on drizzle formation in stratocumulus: implications for cloud radiative properties. *J. Atmos. Sci.* **56,** 4100–4117 (1999).
76. Charlson, R. J. *et al.* Reshaping the theory of cloud formation. *Science* **292,** 2025–2026 (2001).
77. Feingold, G. & Chuang, P. Y. Analysis of the influence of film-forming compounds on droplet growth: implications for cloud microphysical processes and climate. *J. Atmos. Sci,* **59,** 2006–2018 (2002).
78. Rosenfeld, D. & Woodley, W. L. K. Deep convective clouds with sustained supercooled liquid water down to –37.5 °C. *Nature* **405,** 440–442 (2001).
79. Khain, A. P., Rosenfeld, D. & Pokrovsky, A. Simulating convective clouds with sustained supercooled liquid water down to –37.5 °C using a spectral microphysics model. *Geophys. Res. Lett.* **28,** 3887–3890 (2001).
80. Alpert, P. *et al.* Quantification of dust-forced heating of the lower troposphere. *Nature* **395,** 367–370 (1998).
81. Claquin, T. *et al.* Uncertainties in assessing radiative forcing by mineral dust. *Tellus* **50B,** 491–505 (1998).
82. Kaufman, Y. J. *et al.* Satellite and ground-based radiometers reveal much lower dust absorption of sunlight than used in climate models. *Geophys. Res. Lett.* **28,** 1479–1483 (2001).
83. Bond, T. C., Charlson, R. J. & Heintzenberg, J. Quantifying the emission of light-absorbing particles: measurements tailored to climate studies. *Geophys. Res. Lett.* **25,** 337–340 (1998).
84. Christopher, S. A. *et al.* First estimates of the radiative forcing of aerosol generated from biomass burning using satellite data. *J. Geophys. Res.* **101,** 21265–21273 (1996).
85. Li, Z. & Kou, L. Atmospheric direct radiative forcing by smoke aerosols determined from satellite and surface measurements. *Tellus* **50B,** 543–554 (1998).
86. Collins, W. D. *et al.* Simulating aerosols using a chemical transport model with assimilation of satellite aerosol retrievals: methodology for INDOEX. *J. Geophys. Res.* **106,** 7313–7336 (2001).
87. Satheesh, S. K. *et al.* A model for the natural and anthropogenic aerosols over the tropical Indian Ocean derived from Indian Ocean Experiment data. *J. Geophys. Res.* **104,** 27421–27440 (1999).
88. Remer, L. A. *et al.* Urban/industrial aerosol: ground based sun/sky radiometer and airborne in situ measurements. *J. Geophys. Res.* **102,** 16849–16859 (1997).
89. Chou, M. D. A solar-radiation model for use in climate studies. *J. Atmos. Sci.* **49,** 762–772 (1992).
90. Liu M., & Westphal, D. L. A study of the sensitivity of simulated mineral dust production to model resolution. *J. Geophys. Res.* **106,** 18099–18112 (2001).
91. Fraser, R. S., Kaufman, Y. J. & Mahoney, R. L. Satellite measurements of aerosol mass and transport. *Atmos. Environ.* **18,** 2577–2584 (1984).
92. Hsu, N. C., Herman, J. R. & Weaver, C. Determination of radiative forcing of Saharan dust using combined TOMS and ERBE. *J. Geophys. Res.* **105,** 20649–20661 (2000).
93. Torres O. *et al.* A long-term record of aerosol optical depth from TOMS observations and comparison to AERONET measurements. *J. Atmos. Sci.* **59,** 398–413 (2002).
94. Chu, D. A. *et al.* Validation of MODIS aerosol optical depth retrieval over land. *Geophys. Res. Lett.* (in the press).
95. Remer, L. A. *et al.* Validation of MODIS aerosol retrieval over ocean. *Geophys. Res. Lett.* (in the press).
96. Kaufman, Y. J. *et al.* Remote sensing of tropospheric aerosol from EOS-MODIS over the land using dark targets and dynamic aerosol models. *J. Geophys. Res.* **102,** 17051–17067 (1997).
97. Fraser, R. S. & Kaufman, Y. J. The relative importance of aerosol scattering and absorption in remote sensing. *IEEE J. Geosci. Rem. Sens.* **GE-23,** 525–633 (1985).
98. Fouquart, Y. *et al.* Observations of Saharan aerosols: results of ECLATS field experiment. II: Broadband radiative characteristics of the aerosols and vertical radiative flux divergence. *J. Clim. Appl. Meteorol.* **25,** 28–37 (1986).
99. Mishchenko, M. I. & Travis, L. D. Satellite retrieval of aerosol properties over the ocean using polarization as well as intensity of reflected sunlight. *J. Geophys. Res.* **102,** 16989–17013 (1997).
100. Chowdhary, J., Cains, B. & Travis, L. D. Case studies of aerosol retrieval over the ocean from multiangle, multispectral photopolarimetric remote sensing data. *J. Atmos. Sci.* **59,** 383–397 (2002).

Acknowledgements

We thank F. M. Bréon, M. Chin, O. Dubovik, G. Feingold, P. Formenti, M. Herman, D. Herring, B. N. Holben, S. Mattoo, L. Remer and D. Rosenfeld for measurements and calculations used in this paper and for editorial comments. POLDER was a CNES/NASDA project; TOMS and MODIS are NASA projects.